

# Sedimentation of granular columns in the viscous and weakly inertial regimes

Hamza Chraïbi\*<sup>1</sup> and Yacine Amarouchene\*<sup>1</sup>

*1 : Univ. Bordeaux, LOMA,  
UMR 5798, F-33400 Talence, France.  
CNRS, LOMA, UMR 5798, F-33400 Talence, France.*

(Dated: June 6, 2022)

We investigate the dynamics of granular columns of point particles that interact via long-ranged hydrodynamic interactions and that fall under the action of gravity. We investigate the influence of inertia using the Green function for the Oseen Equation. The initial conditions (density and aspect ratio) are systematically varied. Our results suggest that universal self similar laws may be sufficient to characterize the temporal and structural evolution of the granular columns. A characteristic time above which an instability is triggered (that may enable the formation of clusters) is also retrieved and discussed.

Granular materials that are assemblies of discrete macroscopic solid particles with sizes large enough that Brownian motion is irrelevant, have been a subject of intensive research during the past few year [1]. They are ubiquitous in our everyday lives and remain at the heart of several geophysical (sand dunes, coastal geomorphology, avalanches...) and industrial processes (chemical, pharmaceutical, food, agricultural...) [1]. The variety of these fields make these granular materials subject to very different flow and stress conditions. In particular, when the particles are suspended in a fluid, one may expect that subtle hydrodynamic effects should play a leading role [2]. This must be contrasted with the case of dry granular materials for which the influence of the carrying fluid is negligible. In that case both the inelasticity of the collisions and/or the friction between the grains are crucial [1]. While the falling of a single or couple of particles in purely viscous and weakly inertial regimes was well described by Stokes and Oseen [3], understanding the interactions of a cloud of particles remains a challenge, as complex collective dynamics emerge due to the multiple long ranged interactions (see fluidized beds [4, 5]). Similar difficulties exist also for n-body gravitational problems. Therefore, many investigations were led in order to better understand the behavior of these particle laden flows, presenting a large panel of geometries like jets, streams, drops, spherical clouds. The sedimentation of spherical clouds of particles, in an external fluid of variable viscosity, has been recently investigated experimentally and numerically [6]. At the exception of the experimental work of Nicolas [7], investigations related to jets or column of particles focused mainly on highly viscous fluids (i.e. zero Reynolds numbers limit) [8, 9], air and moderate vacuum (Large Reynolds numbers limit) [10–12] or other kinds of interactions : capillary bridges, Wan Der Waals forces [13–16]...

In this letter, we present an investigation that fully characterizes, using point-particle simulations, the

dynamics of freely falling granular columns in different flow regimes, clarifying the dependence to the Reynolds number, the aspect ratio and the particle density.

The main characteristics of the present system are: (i) solid particles suspended in a viscous fluid, and interacting by virtue of the fluid, (ii) particles heavier than the fluid, thus sedimenting on account of gravity. (iii) No continuous supply of particles in the granular cylinder.

We will first describe the model used for the numerical simulations, defining the characteristic quantities of the problem and its relevant parameters before presenting and discussing our results.

At the beginning of the simulation, we randomly initialize the positions of  $N_0$  particles in a cylindrical column of radius  $R_0$  and length  $H_0$ , such as the dimensionless particle density  $n_0 = N_0/(\pi h^*)$  is homogeneous ( $h^* = H_0/R_0$ ). In addition to their settling velocity  $U_\eta = F/(6\pi\eta a)$  in the fluid of viscosity  $\eta$  under the action of the gravitational force  $F$ , the point particles of radius  $a$  are subject to the hydrodynamic pairwise interactions modeled by the dimensionless Green function of the Oseen Equation [2, 3, 6] which represents the additional velocity induced on a point particle by another point particle distant by  $\mathbf{d} = (d_x, d_y, d_z)$  :

$$u_k^* = \frac{3}{4}a^* \left( \frac{d_k}{d^2} \left[ \frac{2l^*}{d}(1-E) - E \right] + \frac{E}{d} \delta_{kz} \right) ; k = x, y, z \quad (1)$$

$$E = \exp \left( -\left(1 + \frac{d_z}{d}\right) \frac{d}{2l^*} \right) ; a^* = a/R_0 ; l^* = \eta/(U_\eta \rho_f R_0) \quad (2)$$

In equation (1), all lengths and velocities were made dimensionless using  $U_\eta$  as a reference velocity and  $R_0$  as a reference length. A reference time  $\tau_\eta = R_0/U_\eta$  was also defined.  $\rho_f$  is the mass density of the external fluid and  $l^*$  represents the importance of the viscous effects. Note that the velocity given by equation (1) is solution to the corrected Navier-Stokes Equation, which models

the weakly inertial regime:

$$\rho_f(\mathbf{U}_\eta \cdot \mathbf{grad})\mathbf{u} = -\mathbf{grad}p + \eta\Delta\mathbf{u} \quad (3)$$

where  $p$  is the fluid pressure.

By choosing the frame of reference moving with the terminal settling velocity of an isolated particle, we compute all the  $N_0 - 1$  interactions on each particle and obtain a set of equations describing the motions of the particles, of the form :

$$\frac{dM_{ki}}{dt} = \sum_{j \neq i} u_k^* \quad k = x, y, z \quad i = 1, N_0 \quad j = 1, N_0 \quad (4)$$

This equation is integrated using an Adams-Bashford time-marching algorithm and at each iteration, we obtain the Cartesian position  $M = (x, y, z)$  of each particle. The detection of the interface of a granular column is performed by dividing axially the domain into  $h^*$  overlapping volumes. For each volume, the radial position of the interface is calculated by calculating the mean radial position of the farthest particles. The parameters for the simulations are the aspect ratio  $h^*$ , the particle density  $n_0$ ,  $l^*$  and  $a^*$ . However, one can notice that equation (1) is linear with respect to  $a^*$  and therefore the dynamics of the problem will vary linearly with it. As a consequence, we set  $a^* = 0.05$  for all simulations. As our simulations neglect particle-particle collisions they are only applicable to dilute regimes.

It is interesting to write the particle Reynolds number such as  $Re_p = a^*/l^* = aU_\eta\rho_f/\eta$  which variation in this problem is performed by varying  $\eta$ , however as we are investigating the behavior of a macroscopic object, we have to define a macroscopic Reynolds number  $Re = R_0U_{col}\rho_f/\eta$ , where  $U_{col}$  is the characteristic velocity of a cylindrical column.  $U_{col}$  can be defined using the settling velocity of a vertical cylinder of aspect ratio  $h^*$  in a viscous fluid, hence  $U_{col} = P \ln(h^*/2)/(2\pi\eta H_0)$ ,  $P$  being the macroscopic gravitational force. Calculating the equivalent mass of the column from its volume fraction, one can find that  $U_{col} = 3\pi n_0 a^* \ln(h^*/2)U_\eta$  and therefore  $Re = 3\pi n_0 \ln(h^*/2)Re_p$ .

An example of simulations performed varying  $Re$  are shown in figure 1. We can first observe that while they fall, all the columns stretch and thin. We can also observe that a leading mushroom shaped plume forms at the front [8] while a particle leakage can be observed at the rear. For the last instant, we can see that the columns lose their cohesion and eventually detach into shorter columns and droplets, which means that a varicose instability grows in time. Considering now the effect of the Reynolds number in relative frames, we can see that increasing  $Re$  relatively slows down the falling of the columns and increases their effective cohesion. We can also observe that size of the leading mushroom is larger for a same instant. It is important to understand

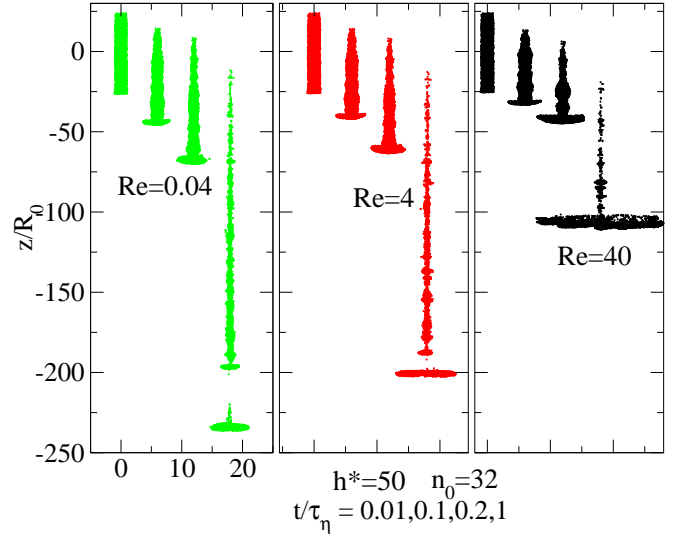


FIG. 1. (Color online) Falling of cylindrical granular columns for  $Re = 0.04$ , 4 and 40 with an aspect ratio  $h^* = 50$  and particle density  $n_0 = 32$ . Four different instant are shown such as  $t/\tau_\eta = 0.01, 0.1, 0.2$  and 1, and time increases from left to right. The columns are shown in the reference frame of an isolated particle falling at its settling velocity.

that, in order to compare them, columns for different  $Re$  were represented in different frames. As the viscosity of the fluid for  $Re = 0.05$  is much larger than the viscosity for  $Re = 50$ , columns at large  $Re$  in the absolute frame will experience a faster dynamics. These results are qualitatively comparable to those of Pignatel [6], which showed that increasing  $Re$  enhances effective cohesion and slows the falling of spherical clouds of particles.

Figure 2 shows the time variation of the center of mass  $V_{mass}$  reduced by a corrected characteristic velocity of the column  $U_{cyl}$ . Indeed, when varying  $Re_p$  at fixed  $h^*$  and  $n_0$ , we observed a correction in  $V_{mass}$  which was not taken into account in  $U_{col}$ . This correction is shown in the inset of figure 2, where  $V_{mass}/U_\eta$  decreases with  $Re_p$  following a logarithmic behavior. We successfully retrieved this behavior by the function  $f(Re_p) = 1/(1 + \ln(1 + l^{*-1})) = 1/(1 + \ln(1 + Re_p/a^*))$  and in order to take into account the  $Re_p$  dependence of the dynamics, we defined a new characteristic velocity  $U_{cyl} = 3\pi U_\eta n_0 a^* \ln(h^*/2) f(Re_p)$  along with a macroscopic characteristic time  $\tau_{cyl} = H_0/U_{cyl}$ . Finally, we can observe in figure 2 that for a large set of different parameters, all the temporal evolution of  $V_{mass}/U_{cyl}$  collapse in a single universal curve. It shows that for  $t \ll \tau_{cyl}$ , the column fall with a constant velocity  $U_{cyl}$  before decreasing with time following a logarithmic behavior when  $t \gg \tau_{cyl}$ . This confirms that  $U_{cyl}$  and  $\tau_{cyl}$  are the adequate velocity and characteristic time that describe the falling of the columns.

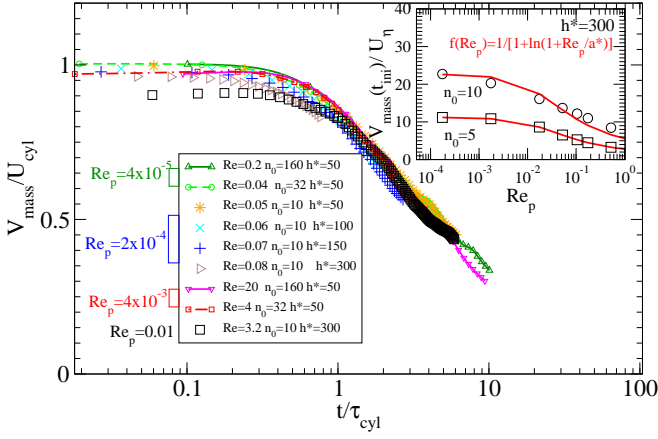


FIG. 2. (Color online) Variation of the reduced velocity of the center of mass  $V_{mass}/U_{cyl}$  versus reduced time  $t/\tau_{cyl}$  for  $Re_p = 4 \times 10^{-5}, 2 \times 10^{-4}, 4 \times 10^{-3}$  and  $10^{-2}$ ,  $h^* = 50, 100, 150, 300$  and  $n_0 = 10, 32, 160$ ;  $U_{cyl} = U_{col}/(1 + \ln(1 + Re_p/a^*))$  and  $\tau_{cyl} = H_0/U_{cyl}$ . Inset: variation of dimensionless initial velocity of the center of mass  $V_{mass}/U_\eta$  versus  $Re_p$  for  $n_0 = 5, 10$  and  $h^* = 300$  (symbols : simulations, line : analytical function).

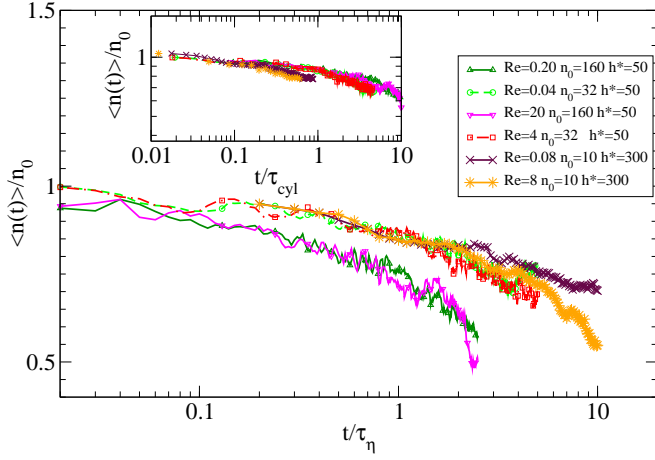


FIG. 3. (Color online) Variation of the reduced particle mean density  $\langle n(t) \rangle / n_0$  versus dimensionless time  $t/\tau_\eta$  for  $Re_p = 4 \times 10^{-5}, 4 \times 10^{-3}$  and  $n_0 = 32$  and  $160$ . Inset : Variation of the reduced particle mean density  $\langle n(t) \rangle / n_0$  versus the reduced time  $t/\tau_{cyl}$  for the same parameters.

The variation of particle mean density  $\langle n(t) \rangle / n_0$  versus dimensionless time  $t/\tau_\eta$  is presented in figure 3. For different Reynolds number and initial particle densities, we observe a first incompressible regime where  $\langle n(t) \rangle$  is almost constant followed by a weakly compressible regime where the mean particle density experiences a slow time decay. While in the main figure, there seems to be different dynamics, the inset of figure

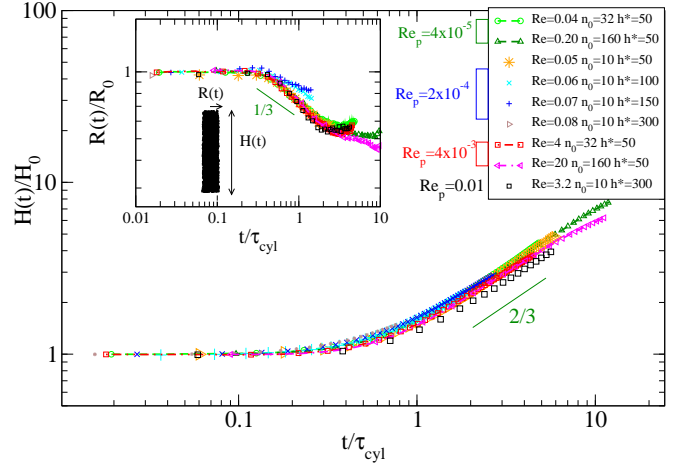


FIG. 4. (Color online) Variation of the reduced length of the column  $H(t)/H_0$  versus reduced time  $t/\tau_{cyl}$  for  $Re_p = 4 \times 10^{-5}, 2 \times 10^{-4}, 4 \times 10^{-3}$  and  $10^{-2}$ ,  $h^* = 50, 100, 150, 300$  and  $n_0 = 10, 32, 160$ . Inset: Variation of the mean reduced radius of the column  $R(t)/R_0$  versus reduced time  $t/\tau_{cyl}$  for the same set of parameters.

3 shows that using the characteristic time  $\tau_{cyl}$  provides a better collapse of the data. In addition, we can see that  $t \ll \tau_{cyl}$  corresponds to an incompressible regime while  $t \gg \tau_{cyl}$  corresponds to a weakly compressible flow.

The deformations of the columns are displayed in figure 4. It provides an adequate description of the dynamics of both the reduced length  $H(t)/H_0$  and of the reduced mean radius  $R(t)/R_0$  (calculated excluding the extremities of the column). Once again, the dynamics of the column deformation for a large set of different parameters  $h^*$ ,  $n_0$  and  $Re_p$  are represented by universal curves. When  $t \ll \tau_{cyl}$  the columns remain undeformed while for  $\tau_{cyl} < t < 10\tau_{cyl}$ , the length increases following a universal scaling such as  $H(t) \sim H_0(t/\tau_{cyl})^{2/3}$  and the mean radius decreases such as  $R(t) \sim R_0(t/\tau_{cyl})^{-1/3}$ . Assuming a weakly compressible flow for  $t > \tau_{cyl}$  (in agreement with figure 3), the volume of the column has to remain constant, i.e.  $\pi R(t)^2 H(t) \sim \pi R_0^2 H_0$  which is well recovered by the previous scaling laws.

Now let us focus on the strain rate  $dV_z/dz$  selected at a local scale. It is an important parameter to describe the elongational stretching applied to the columns. It is known that stretching stabilizes liquid columns and prevent instabilities from growing and forming satellite drops [17]. Figure 5 provides a universal curve representing the variation of the reduced axial velocity gradient  $(dV_z/dz)/(n^*U_\eta/H_0)$  versus reduced time  $t/\tau_{cyl}$  where different set of parameters present a good collapse. The elongation rate, or axial velocity gradient (which extent grows with time along the column), is deduced from the axial velocities of the particles at the rear of the columns, as shown in the inset. We can

clearly see that in the incompressible regime ( $t < \tau_{cyl}$ ), the elongational rate remains constant and scales like  $n^*U_\eta/H_0$ . This scaling comes from the fact that a single particle is on average surrounded by  $2N_0/h^* = n^*$  particles (i.e. the particles contained in a sphere of diameter  $2R_0$ ), therefore its characteristic velocity is  $n^*U_\eta$  while its characteristic axial length is  $H_0$ . In the weakly compressible regime ( $t > \tau_{cyl}$ ),  $dV_z/dz$  decays like  $t^{-1}$ . This is consistent with an incompressible self similar decay of the column radius  $R(t) \sim R_0 t^\alpha$  that gives  $(dV_z/dz) = -\frac{2}{R} \frac{dR}{dt} \sim t^{-1}$  independently of the thinning exponent  $\alpha$ . Although not strictly comparable as they perform event-driven simulations of streams of particles interacting via collisions and cohesive forces and not via hydrodynamic interactions, Ulrich and Zippelius [16] showed a similar result in the case of particles that fall in vacuum under the action of gravity. In that case the elongational rate is simply retrieved from the incompressibility condition and the velocity field imposed by the free fall. Finally, figure 5 also displays snapshots of columns at different Reynolds number. We observe that for  $t \ll \tau_{cyl}$ , the column are cohesive and destabilization has not yet occurred, while the columns for  $t > \tau_{cyl}$  show a clear destabilization due to the development of a varicose instability.

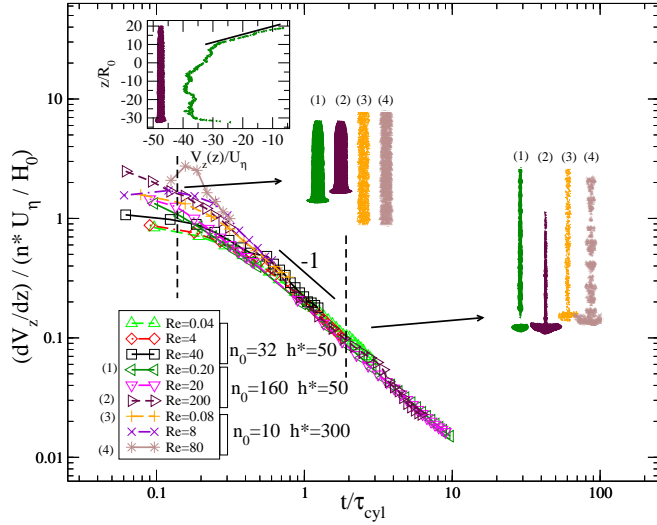


FIG. 5. (Color online) Variation of the reduced axial velocity gradient  $(dV_z/dz)/(n^*U_\eta/H_0)$  versus reduced time  $t/\tau_{cyl}$  for  $Re = 0.04 \dots 200$ ,  $h^* = 50, 300$  and  $n_0 = 10, 32, 160$ ;  $n^* = 2\pi n_0$ . Inset: Shape of a column (left) axial position  $z/R_0$  versus particle axial velocity  $V_z$  (right). The black line, shows the linear behavior of  $V_z$  with  $z$ .

Finally, let us focus on the description of the instability that leads to the destabilization of the columns. The main features of the instability are shown in figure 6. In the main panel of figure 6, we can note that the value of

the most unstable wavelength  $\lambda$  is almost constant and shows no clear dependence on the Reynolds number ( $\lambda$  was deduced from the interface profile). In the regime  $Re \ll 1$ , we found  $\lambda \sim 15R_0$  for  $n_0 = 5$  and  $\lambda \sim 12R_0$  for  $n_0 = 10$  which are both consistent with the values found in earlier investigations [8, 9] dedicated to the effect of  $n_0$ . The inset of figure 6 shows the temporal evolution of the standard deviation of the reduced radial variation (excluding the front drop)  $\sigma n_0^{1/2}$  for  $n_0 = 5$  and 10 and for  $Re = 0.08, 0.8, 8$ . We can see that the data collapse for  $Re \ll 1$ , in good agreement with Crosby and Lister who suggested that the growth of the standard deviation of the reduced radial variation are mainly due to fluctuations in the average number density of particles along the axial distance about its mean value [9]. However,  $\sigma$  seems to present larger values for  $Re \gg 1$ . This means that increasing the Reynolds number may have a noticeable effect on the varicose instability. This induces a stronger effective cohesion and leads to a more efficient destabilization. These observations provide another route to the instability of granular jets along with the recently observed clustering due to cohesion and liquid bridges between grains [14, 15]. Furthermore, our results suggest that the sedimentation of particle-laden jets may eventually furnish an interesting system to study the compressible Rayleigh-Plateau instability as suggested recently [18].

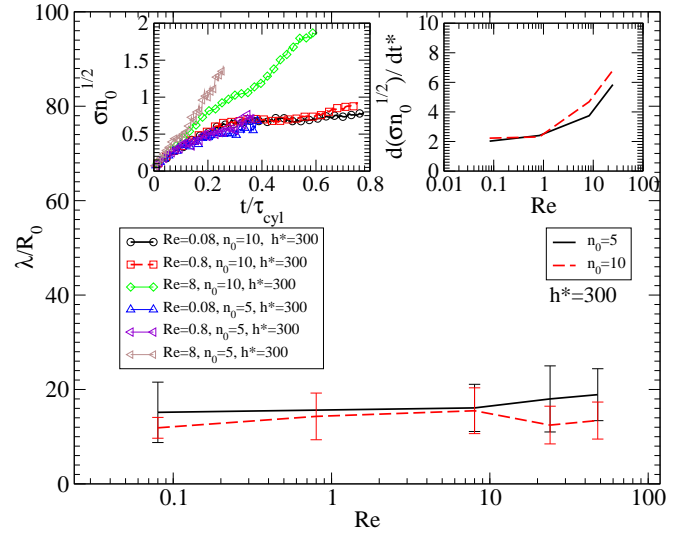


FIG. 6. (Color online) Variation of the reduced most unstable wavelength  $\lambda/R_0$  versus  $Re$  for  $n_0 = 5, 10$  and  $h^* = 300$ . Left inset : Variation of the standard deviation of the radial variation  $\sigma$  versus reduced time  $t/\tau_{cyl}$  for  $n_0 = 5, 10$ ,  $Re = 0.08, 0.8, 8$  and  $h^* = 300$ . Right inset : Variation of  $d(\sigma n_0^{1/2})/dt^*$  (calculated at short times) versus  $Re$  for  $n_0 = 5, 10$  and  $h^* = 300$ .  $t^* = t/\tau_{cyl}$ .

To conclude, we have shown that universal scaling laws fully characterize the dynamics of free falling granular columns in viscous fluids. The characteristic velocity  $U_{cyl}$  scales linearly with the particle density, while it shows a logarithmic increase with the aspect ratio and a decreasing logarithmic correction with the particle Reynolds number. A universal characteristic time  $\tau_{cyl}$  based on  $U_{cyl}$  and the column length  $H_0$  has also been retrieved. When  $t < \tau_{cyl}$ , the flow could be considered as incompressible, and the columns deform only slightly and are subjected to a constant strain rate  $n^*U_\eta/H_0$  while falling at a constant velocity  $U_{cyl}$ . For  $t > \tau_{cyl}$ , we showed that the flow was weakly compressible, and that the columns were subjected to an elongational rate decaying like  $t^{-1}$ , while they stretched like  $t^{2/3}$  and thinned like  $t^{-1/3}$  before the development of a varicose instability leading to a long wavelength destabilization. Finally, we found that the most unstable wavelength of the instability of the order of  $\sim 10R_0$  is almost independent of inertia corrections while the growth rate of the most unstable mode shows a clear increase with the Reynolds number.

### Acknowledgement

We thank Pierre Navarot for the preliminary investigation. This research is supported by CR Aquitaine Grants no. 2006111101035, no. 20091101004 and by ANR Grant no. ANR-09-JCJC-0092.

\* Corresponding authors' e-mails :

h.chraibi@loma.u-bordeaux1.fr

y.amarouchene@loma.u-bordeaux1.fr

- 
- [1] B. Andreotti, Y. Forterre, and O. Pouliquen, *Les milieux granulaires : entre fluide et solide*, EDP Sciences/CNRS Edition (2011) . english translation *Granular Media : Between Fluid and Solid* , Cambridge University Press (2013).
  - [2] E. Guazzelli and Morris J. F., *A physical introduction to suspension dynamics*, Cambridge Texts in Applied Mathematics, Cambridge University Press (2012).
  - [3] J. Happel, and H. Brenner, *Low Reynolds number hydrodynamics*, Springer (2009).
  - [4] R.E . Cafisch and J. H. C. Luke, *Phys. Fluids*. **28**, 759 (1985).
  - [5] E. Guazzelli and Hinch E. J. "Fluctuations and instability in sedimentation", *Annu. Rev. Fluid Mech.* **43**, 97-116 (2011).
  - [6] F. Pignatelli, M. Nicolas & E. Guazzelli, *J. Fluid. Mech.*, **671**, 34, (2011).
  - [7] M. Nicolas, *Phys. Fluids*. **14**, 3570, (2002).
  - [8] F. Pignatelli, M. Nicolas, E. Guazzelli & D. Saintillan, *Phys. Fluids*, **21**, 123303, (2009).
  - [9] A. Crosby & J. R. Lister, *Phys. Fluids*, **24**, 123101, (2012).
  - [10] Y. Amarouchene, J-F Boudet & H. Kellay, *Phys. Rev. Lett.* **100**, 218001, (2008).
  - [11] G. Prado, Y. Amarouchene & H. Kellay, *Phys. Rev. Lett.* **106**, 198001 (2011).
  - [12] G. Prado, Y. Amarouchene & H. Kellay, *Europhysics Lett.* **102**, 24006 (2013).
  - [13] M. E. Möbius, *Phys. Rev. E*. **74**, 051304 (2006).
  - [14] J. R. Royer, D. J. Evans, L. Oyarte, Q. Guo, E. Kapit & M. E. Möbius and S. R. Waitukaitis and H. M. Jaeger, *Nature*. **459**, 11010 (2009).
  - [15] S. R. Waitukaitis, H. F. Grütjen, J. R. Royer & H. M. Jaeger, *Phys. Rev. E*. **83** 051302 (2011).
  - [16] S. Ulrich & A. Zippelius, *Phys. Rev. Lett.* **109**, 166001 (2012).
  - [17] J. Eggers, E. Villermaux *Physics of liquid jets* , *Rep. Prog. Phys.* **71** , 036601 (2008).
  - [18] U. Miyamoto, *J. Fluid Mech.* **700**, 441 (2012).